

PAPER

Optimizing extrusion-based 3D bioprinting of plant cells with enhanced resolution and cell viability

To cite this article: Dezhi Zhou *et al* 2025 *Biofabrication* **17** 025008

View the [article online](#) for updates and enhancements.

You may also like

- [Lung dECM matrikine-based hydrogel reverses bleomycin-induced pulmonary fibrosis by suppressing M2 macrophage polarization](#)
Xinglong Zhu, Ying Yang, Shengqiang Mao et al.
- [Volumetric bioprinting of the osteoid niche](#)
Jessie Duquesne, Laurens Parmentier, Edward Vermeersch et al.
- [Systematic development and bioprinting of novel nanostructured multi-material bioinks for bone tissue engineering](#)
Jannika T Korkeamäki, Ahmad Rashad, Miina Ojansivu et al.

Biofabrication



PAPER




Optimizing extrusion-based 3D bioprinting of plant cells with enhanced resolution and cell viability

RECEIVED
5 August 2024

REVISED
8 December 2024

ACCEPTED FOR PUBLICATION
23 January 2025

PUBLISHED
5 February 2025

Dezhi Zhou(周德志)^{1,3,4,6} , Peixi Li(李佩锡)^{1,3,4,6}, Shuang Yu(余爽)^{1,3,4} , Zhenhua Cui(崔镇华)^{1,3,4},
Tao Xu(徐弢)⁵ and Liliang Ouyang(欧阳礼亮)^{1,2,3,4,*} 

¹ Biomufacturing Center, Department of Mechanical Engineering, Tsinghua University, Beijing 100084, People's Republic of China

² Tsinghua University, Beijing 100084, People's Republic of China

³ Biomufacturing and Rapid Forming Technology Key Laboratory of Beijing, Beijing 100084, People's Republic of China

⁴ Biomufacturing and Engineering Living Systems Innovation International Talents Base (111 Base), Beijing 100084, People's Republic of China

⁵ Research Institute of Tsinghua University in Shenzhen, Shenzhen 518057, People's Republic of China

⁶ Co-first authors.

* Author to whom any correspondence should be addressed.

E-mail: ouy@tsinghua.edu.cn

Keywords: plant cells, bioprinting, plant cell immobilization, cell printing, parameter optimization

Supplementary material for this article is available [online](#)

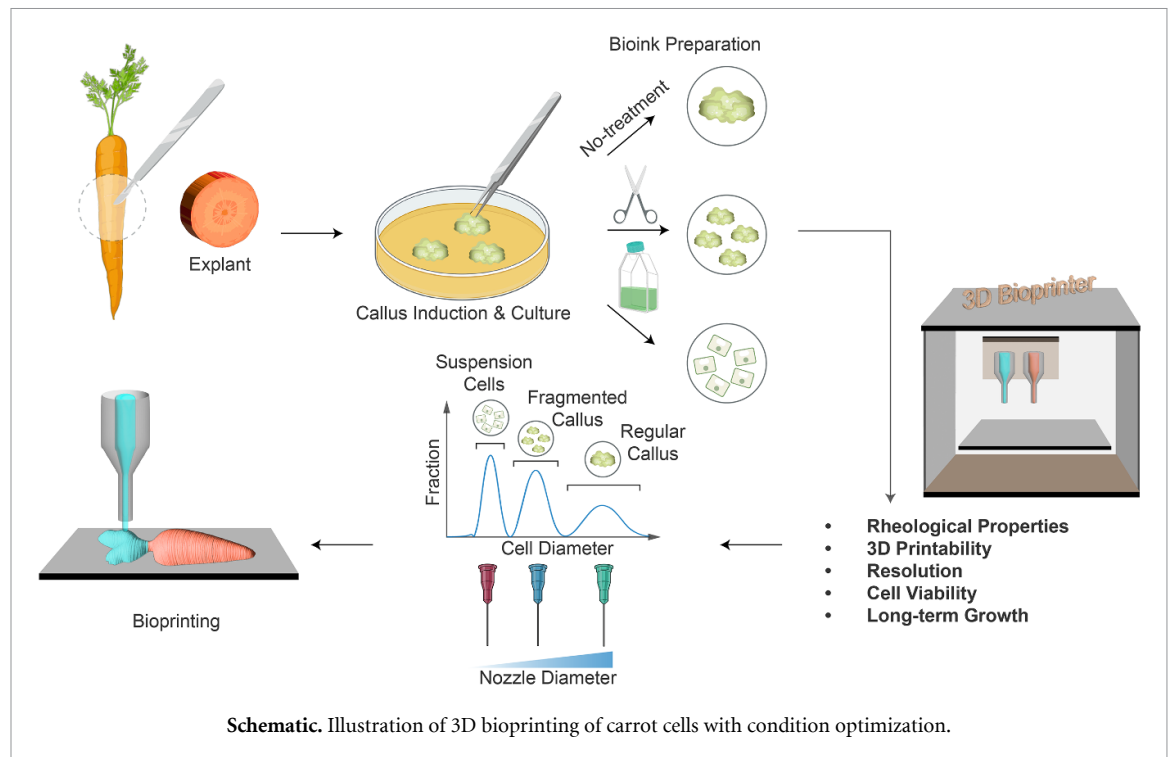
Abstract

3D bioprinting of plant cells has emerged as a promising technology for plant cell immobilization and related applications. Despite the numerous progress in mammalian cell printing, the bioprinting of plant cells is still in its infancy and needs further investigation. Here, we present a systematic study on optimizing the 3D bioprinting of plant cells, using carrots as an example, towards enhanced resolution and cell viability. We mainly investigated the effects of cell cluster forms and nozzle size on the rheological, extrusion, and printability properties of plant cell bioinks, as well as on the resultant cell viability and growth. We found that when the printing nozzle is larger than 85% of the cell clusters embedded in the bioink, smooth extrusion and good printability can be achieved together with considerable cell viability and long-term growth. Specifically, we optimized a bioink composited with suspension-cultured carrot cells, which exhibited better uniformity, smoother extrusion, and higher cell viability over 1 month culture compared to those with the regular callus or fragmented callus. This work provides a practical guideline for optimizing plant cell bioprinting from the bioink development to the printing outcome assessment. It highlights the importance of selecting a matched nozzle and cell cluster and might provide insights for a better understanding and exploitation of plant cell bioprinting.

1. Introduction

Plant cell immobilization has been introduced to enhance the biotransformation of compounds for decades [1]. Under the immobilization conditions, plant cells can continuously produce secondary metabolites without needing cell removal to collect purified products [2]. It has also been demonstrated that some fragile plant cells cultured in immobilized mode can be protected with an enhanced survival rate and increased metabolite production compared to suspension culture [3, 4]. Recently, advanced biofabrication technologies, such as 3D bioprinting,

have been introduced to the field of plant cell culture, which further adds the value of structural customization to conventional plant cell immobilization. In 2015, Lode and colleagues first introduced the concept of green bioprinting by extrusion printing microalgae in a spatially organized manner and cultivated them over 12 d [5, 6], followed by an extension to land plant cells in 2017 [7]. Since then, plant cell bioprinting has been believed to be promising in different applications, such as high-value compound biomanufacturing [8, 9], customized wood [10, 11] and food production [12, 13], and cell-microenvironment interaction studies [14].



The extrusion-based 3D bioprinting is currently the most widely used technology for plant cell printing, where plant cells are embedded in a hydrogel matrix to formulate a plant bioink for extrusion printing into 3D structures. Like mammalian cell bioprinting, high shear stress accompanying the extrusion process might cause irreversible damage to the plant cells [15]. The cell walls could potentially protect cells, but the large vacuoles of plant cells add to the sensitivity to shear stress [16, 17]. Moreover, plant cells usually exhibit nonuniform shapes and tend to aggregate, making it difficult to disperse them in the bioink uniformly. Unlike mammalian cells, plant cells usually present as aggregates in the bioinks. Researchers have attempted to mitigate shear stress on cells by using nozzles with larger inner diameters, such as $\sim 1000\ \mu\text{m}$ nozzle for carrot callus [12], $\sim 840\ \mu\text{m}$ nozzle for transgenic rice cells [9], $\sim 840\ \mu\text{m}$ nozzle for lettuce cells [13], $\sim 770\ \mu\text{m}$ nozzle for tobacco BY-2 cell [8], and $\sim 610\ \mu\text{m}$ nozzle for basil cells [7]. However, a large nozzle usually means poor fabrication resolution. To better present the state of the art, we have collected and summarized all the existing research articles on land plant cell bioprinting, and currently, there are only nine relevant articles to the best of our knowledge (table S1). Indeed, most of the work relies on a large nozzle to adapt to the processing of cell aggregates. Even so, some work still compromises cell survival rate [14] and some others showed live/dead images but no quantitative survival rate data [7, 8, 12, 15]. In a special example, Van den Broeck *et al* disrupted the cell wall and used single protoplasts to formulate the

bioink, which allowed them to use smaller nozzles [14]. The resultant cell survival rate was only $\sim 30\%$ on day 5, which was likely due to the removal of protective walls.

Together, plant cell bioprinting is still in its infancy, requiring further investigation and optimization to refine the process. Specifically, it remains to be investigated how to enhance the printing resolution while maintaining the cell survival rate. Unlike mammal and algae cells, the shape and size of plant cells are highly contingent on their initial callus stage even for those derived from the same region of explant, leading to significant variability in collected callus [18]. This variability complicates the optimization of the bioprinting process, particularly in the selection of printing nozzles, a critical factor that determines printing resolution and cell viability [19].

Here, we systematically optimize the bioprinting process by adapting different forms of plant cells and nozzles of different sizes, using carrot cells as an example (schematic). The objective of this study is to address the trade-off between the printing resolution and the viability of printed plant cells. Cells from physically fragmented callus or suspension-cultured cells are prepared and embedded in the gelatin/alginate composite hydrogel as the bioink, which exhibits excellent printability for bioprinting in both air and suspension bath environments. Compared to the regular callus (R-Callus) and physically fragmented callus (F-Callus) obtained from the solid medium method, the suspension culture method can effectively lower the cell cluster size to nearly single cell (S-Cell) level with enhancing dispersibility.

Consequently, we deem suspension-cultured cells to be optimal cell sources for bioprinting applications. Using a matched nozzle with an inner diameter larger than 85% of cell clusters, the suspension carrot cells can be bioprinted with a narrow nozzle and show remarkable activity during the 35 d culture. Cell survival rate can be obtained to over 80% at day 4 after bioprinting and the encapsulated cells keep stable viability and uniform growth over a one-month culture. Notably, a centimeter-scale carrot-shaped 3D architecture is well fabricated as a proof of concept for large-scale manufacturing potential. Our study not only optimizes the bioprinting of carrot cells with finer filament building blocks and higher cell viability but also provides practical guides and insights for processing other land plant cells, paving the way for advanced plant cell engineering applications.

2. Results and discussion

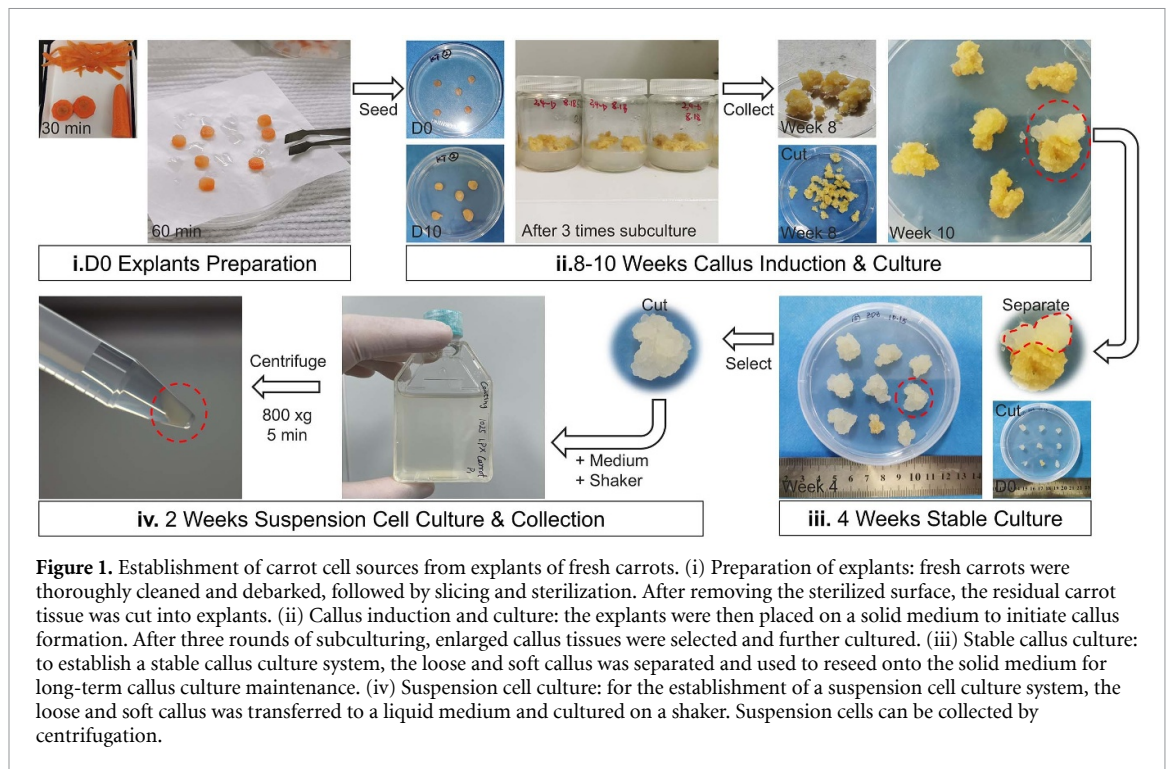
2.1. Preparation of the plant cell-laden bioinks

Three carrot cell clusters derived from the carrot explant (figure 1) were used as cell sources to prepare the bioink (figure 2(a)). The regular callus (R-Callus) was cultured from fresh carrot explants source under solid medium condition. Extruding the regular callus through a series of needles would shear the cell clusters into fragmented callus (F-Callus). When cultured the R-Callus in the suspension medium, nearly single cells (S-Cell) could be obtained. Live/Dead staining indicated considerable cell viabilities for all cell clusters, which were $93.7 \pm 3.1\%$, 85.7 ± 4.9 , and $97.8 \pm 1.9\%$ for R-Callus, F-Callus, and S-Cell, respectively (figure 2(b)). R-Callus exhibited the largest diameter range with a mean diameter of $712 \pm 363 \mu\text{m}$. In contrast, the F-Callus had a mean diameter of $298 \pm 153 \mu\text{m}$, and that of S-Cell was only $174 \pm 79 \mu\text{m}$ (figure 2(c)). These results indicated that the injection treatment and suspension culture could both produce cell clusters with reduced diameter. Similarly, the size distribution of these cell clusters measured by the laser particle analyzer showed a more concentrated distribution in cell cluster size of the S-Cell group than those in the R-Callus and F-Callus groups (supplementary figure 1). To formulate the bioink, cell clusters were dispersed in a hydrogel precursor solution composited of 10 wt% gelatin and 1.5 wt% sodium alginate, with a cell density of 0.12 g ml^{-1} . Realizing that bioink uniformity is pivotal for cell distribution within bioprinted structures, we conducted a transparency test to evaluate the effects of cell types on bioink uniformity. Different types of cells were mixed with a gelatin-alginate solution at an equivalent cell concentration to formulate corresponding bioinks. The callus aggregates were optically visible in the vial. When placing the gels on a lettered background, it was found that the transparency of bioink decreased with an increase in cell cluster diameter (figure 2(d)). Specifically, the

underlying letters were hardly seen through the R-Callus and F-Callus gels, while the letters were visible through the S-Cell gel. To further analyze the uniformity of these formulations, we conducted optical density (OD) measurements of each bioink formulation to evaluate the variance (figure 2(e)). The OD value and its standard deviation of S-Cell were much lower than those of the F-Callus and R-Callus, suggesting that the S-Cell group had a relatively uniform and dispersed cell distribution.

2.2. Rheological characterization and extrusion assessment of the bioinks

A comprehensive rheological assessment is essential to understand the properties of cell-laden bioink and to evaluate printability. Temperature sweeps of cooling and warming were conducted on the three cell-laden bioinks, with acellular hydrogel as a control (figures 3(a) and (b)). The inclusion of regular and fragmented callus in the bioinks would both significantly enhance the shear moduli and lead to a higher storage modulus than loss modulus throughout the tested temperature range ($4 \text{ }^\circ\text{C}$ – $30 \text{ }^\circ\text{C}$) regardless of cooling or warming procedures, without a typical sol-gel transition. Though the presence of suspension-cultured cells also slightly increased the shear modulus at high-temperature regions, the sol-gel transition was more similar to the acellular counterpart. Nevertheless, the storage modulus of all the formulations experienced a distinguishable increase from a steady level at the high-temperature region to higher values at lower temperatures. We defined the temperature point where the storage modulus shifted between a sharp change trend and a stable stage as an equivalent rheological transition point. In the cooling test, both the acellular and cell-laden bioinks (R-Callus, F-Callus, and S-Cell) showed a similar solidifying transition point around $\sim 12 \text{ }^\circ\text{C}$, while a liquifying transition point at $\sim 21 \text{ }^\circ\text{C}$ was observed in the warming procedure. The thermal hysteresis observed between cooling and warming cycles is also reported in other thermosensitive hydrogels and may related to varying energy requirements for the association and disassociation of polymer networks [20]. Shear-thinning behavior of bioink is fundamental for extrusion-based bioprinting, driving us to verify whether the added cells affect the intrinsic shear-thinning behavior of gelatin/alginate composite hydrogel (figure 3(c)). Both the acellular gel and cell-laden bioinks displayed a desirable declining cure of viscosity with an increasing shear rate, indicating their shear-thinning behavior. According to previous studies, the high concentration of either animal cells [15] or yeast cells [21] showed less impact on the rheological properties of bioink. Our results are consistent with a previous report [15] that the inclusion of plant cells can significantly increase the viscosity of bioink. Further, the larger clusters of plant cells could lead to a higher shear stress [15]. Nevertheless, the



bioinks with different forms of plant cells show shear-thinning behaviors.

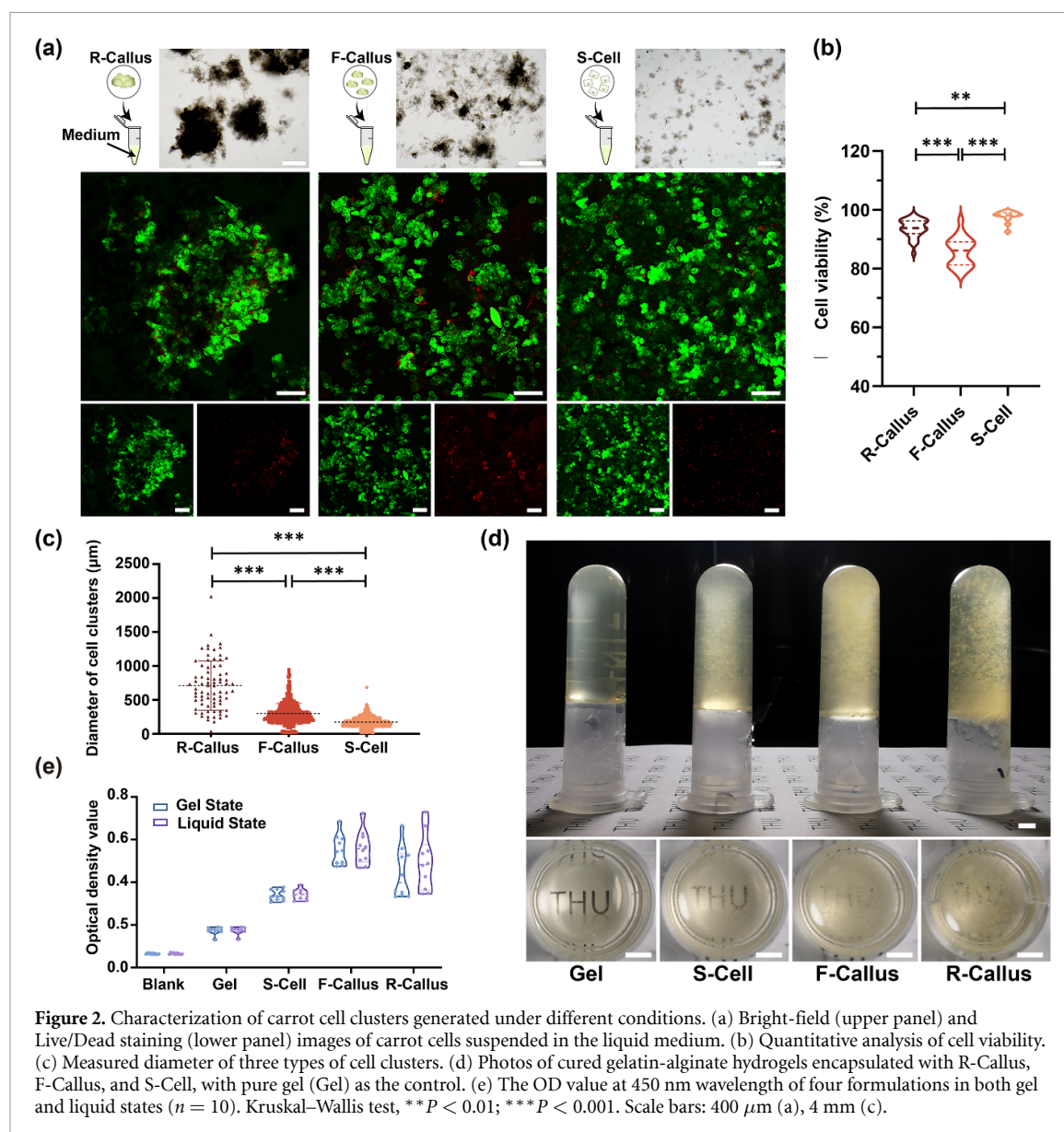
Self-healing of bioink post-extrusion ensures the shape maintenance of extruded filaments for subsequent printing process. To evaluate this capacity, we subjected the bioinks to a 3-step oscillatory test that simulated shearing and restoration processes. All samples exhibited a shear-thinning behavior at high strain (e.g. 1000%) and subsequently restored at low strain (e.g. 1%), suggesting their suitability for extrusion bioprinting (figure 3(d)). Next, we conducted an extrusion experiment to verify the extrusion capacity of bioinks and optimize the extrusion nozzle for each type of bioink (figure 3(e)). The R-Callus bioink was proven to be easily clogged, even using the 18G nozzle (inner diameter of 0.840 mm). This is not surprising, considering the considerable amount of cell clusters that are larger than the nozzle (figure 2(c)). In contrast, the F-Callus bioink could be successfully extruded into hanging filaments with lengths of 58.0 ± 7.6 mm, 47.8 ± 9.2 mm, and 14.7 ± 9.9 mm by using 18G, 22G, and 24G nozzles, respectively. Clogging occurred only with the narrower nozzle (e.g. 27G). The S-Cell bioink produced hanging filaments with lengths of 52.5 ± 2.6 mm, 41.8 ± 2.7 mm, 36.2 ± 2.4 mm, and 9.7 ± 2.2 mm by using 18G, 22G, 24, and 27G nozzles, respectively, while clogging started to occur with the 32G nozzle. Compared to the F-Callus group, the S-Cell group exhibited a more concentrated distribution of filament lengths, potentially related to the uniformity of cell cluster size (figure 2(c)). The uniformity of embedded cells contributes to more consistent extrusion. These results indicated that the size of cell clusters significantly

influences the selection of a printing nozzle and, thus the printing resolution. Utilizing smaller S-Cell clusters as the cell source and a narrower nozzle for bioprinting could potentially enhance the printing resolution.

2.3. Printability of the plant cell-based bioinks

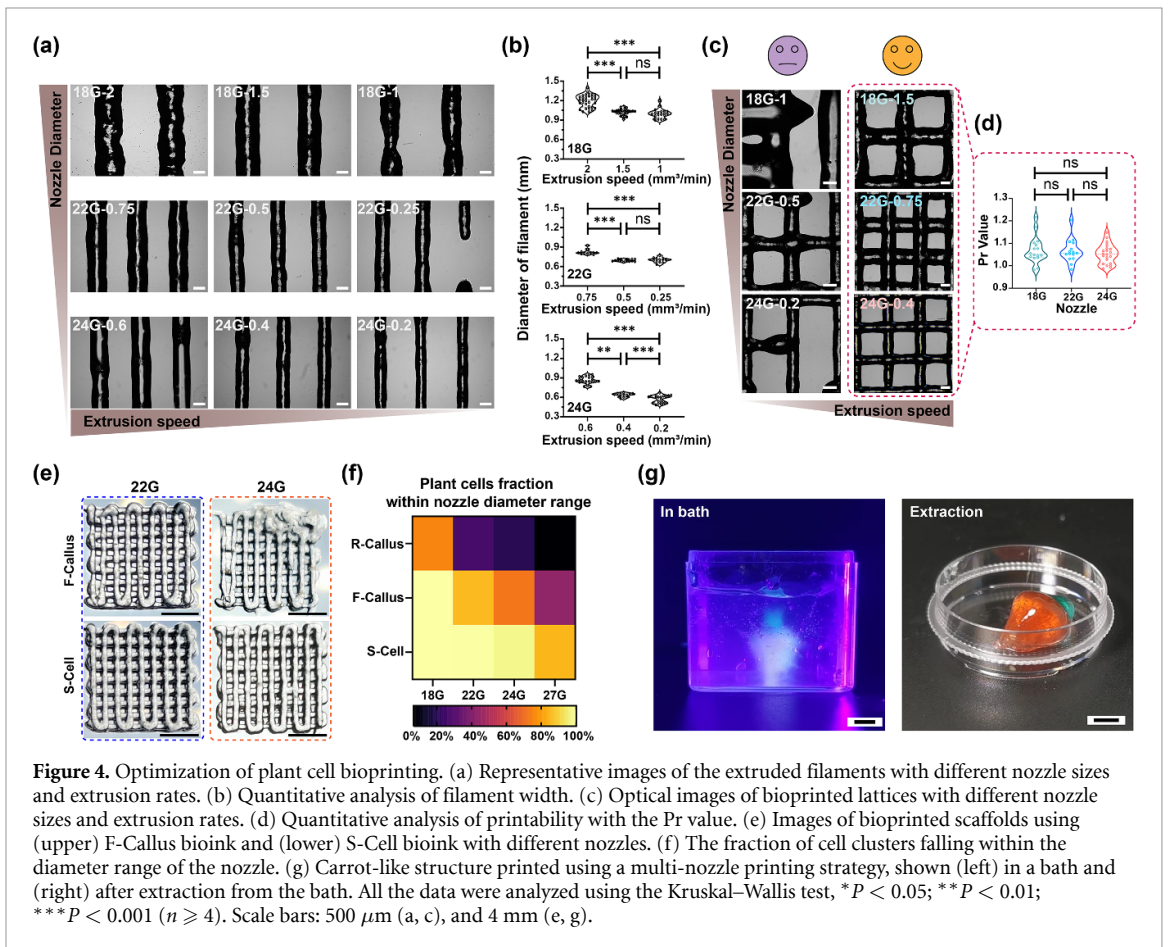
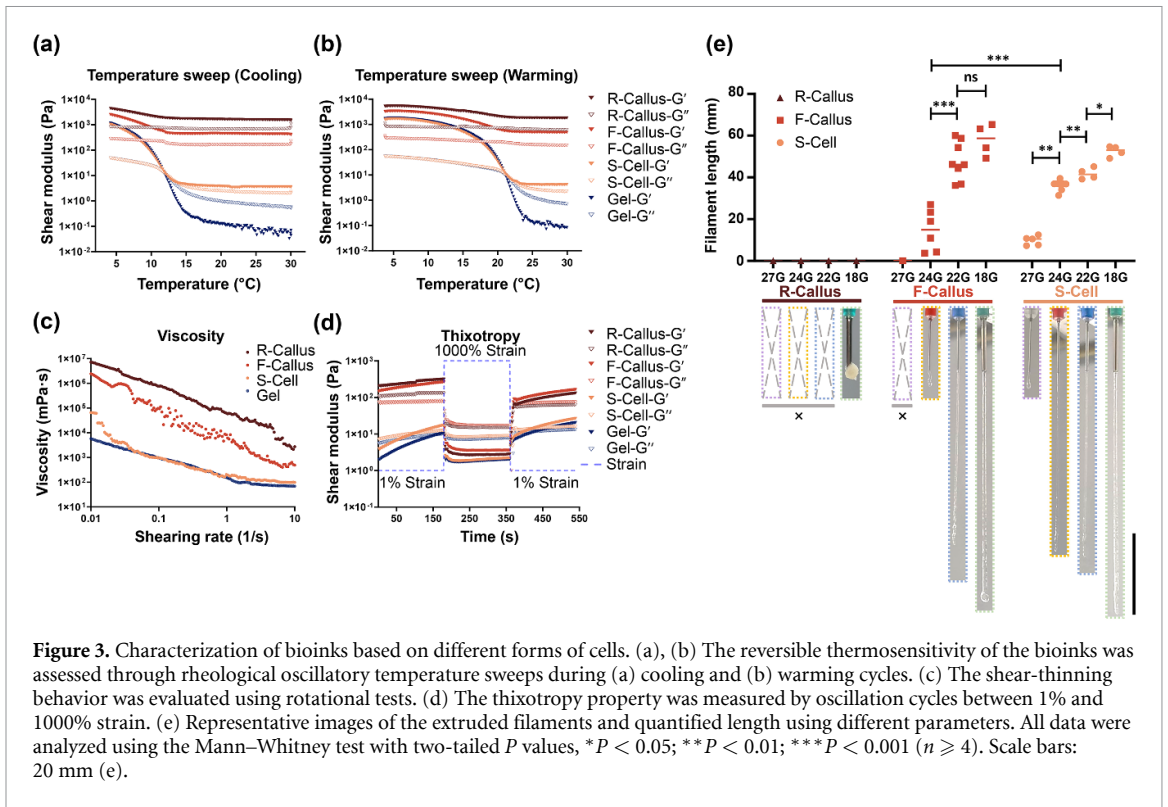
Since the R-Callus bioink cannot be smoothly extruded into hanging filaments with commonly used nozzles, we focused on the comparison of the F-Callus and S-Cell bioinks regarding the bioprinting practice in the following studies. For optimizing bioprinting parameters, we first explored bioprinting S-Cell bioinks with 18G, 22G, and 24G nozzles (figure 4). To study the relationship between extrusion speed and filament diameter, the bioprinter moving speed was fixed at 5 mm s^{-1} for the following experiments. With proper extrusion speed, uniform and smooth filaments could be obtained with 18G, 22G, and 24G nozzles (figure 4(a)), but clogging occurred with a 27G nozzle (supplementary figure 2(a)). The resultant filament diameters for 18G (extrusion speed of $1.5 \text{ mm}^3 \text{ min}^{-1}$), 22G (extrusion speed of $0.75 \text{ mm}^3 \text{ min}^{-1}$), and 24G (extrusion speed of $0.4 \text{ mm}^3 \text{ min}^{-1}$) nozzles were $1025.0 \pm 47.8 \mu\text{m}$, $822.7 \pm 40.7 \mu\text{m}$, and $635.2 \pm 28.8 \mu\text{m}$, respectively, suggesting the feasibility of tuning printing resolution with proper nozzles. Next, we printed a standard lattice structure using these three nozzles, which enabled desirable printability with similar Pr values (figures 4(c) and (d)).

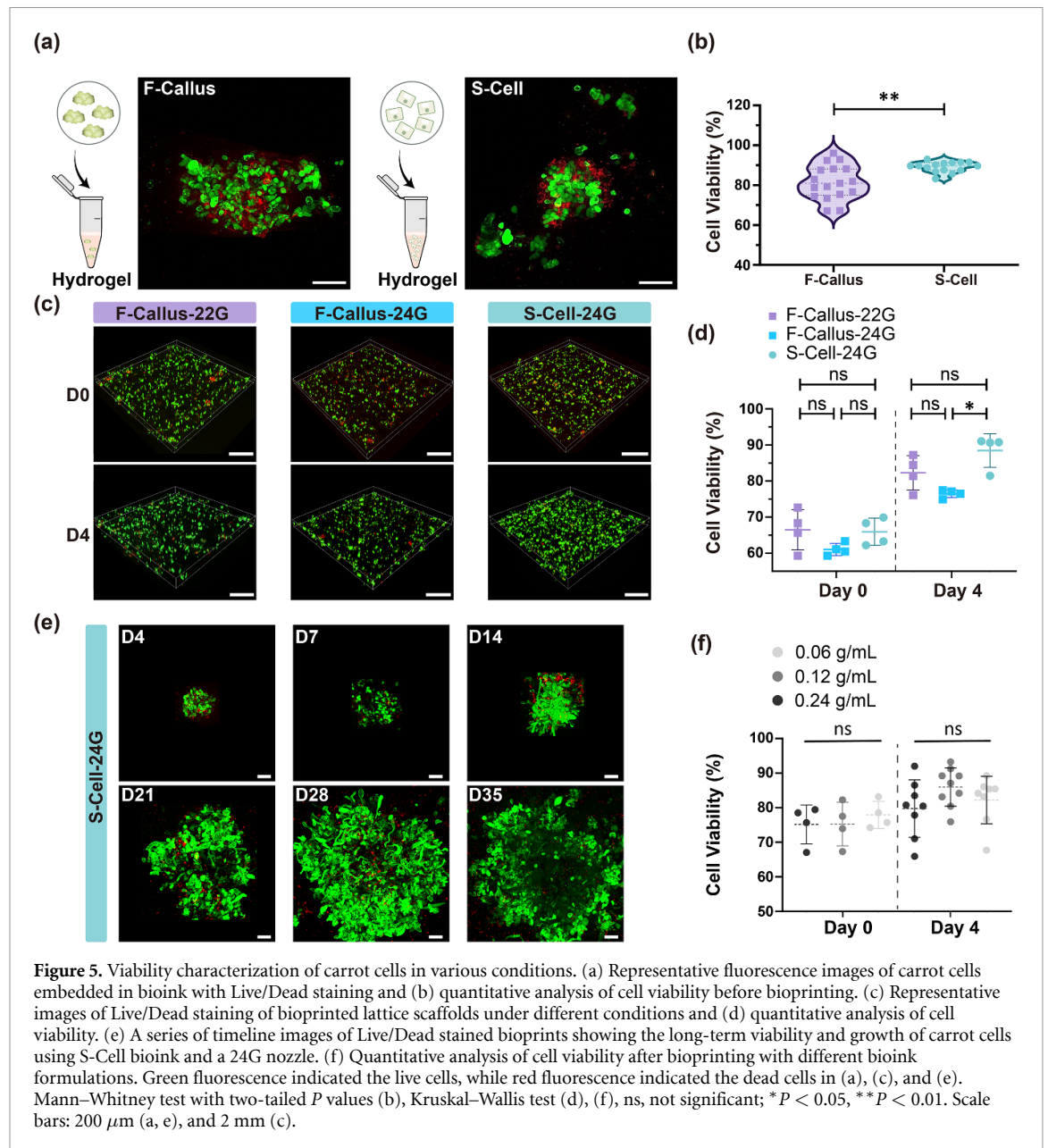
Next, to evaluate the influences of cell types on bioprinting, we printed the bioinks into a standard lattice structure using F-Callus and S-Cell bioinks



with various nozzles of different sizes and assessed their printability (figure 4(e)). The F-Callus bioink produced uniform lattices with a 22G nozzle but encountered partial deformation and filament missing with a 24G nozzle. In contrast, the S-Cell bioink was successfully printed into lattices using both 22G and 24G nozzles, while deformation issues only occurred with the 27G nozzle (supplementary figure 2(b)). These observations suggest that filament missing, and over-extrusion are related to the clogging of bioinks during extrusion, which in turn affects printability. Therefore, selecting a nozzle that matches the size of cell clusters is essential to achieve high-resolution plant cell bioprinting. To generate instructive guidance, we quantified the fraction of cell clusters smaller than the nozzle, which is termed critical fraction (figure 4(f)). The 18G nozzle could cover 75.5% of regular calli and 100% of the other two types of cells. In contrast, less than 27% of regular calli could fit into the 22G nozzle or smaller ones, explaining

the clogging and difficulty of extrusion (figure 3(e)). For the fragmented callus, the critical fractions for 22G, 24G, and 27G were 85.3%, 71.7%, and 43.1%, respectively. In contrast, the critical fractions of suspension cells were above 85% regardless of the nozzle size (27G or larger nozzles). By linking the printability outcomes with the critical fraction data, we can conclude that when more than 85% of cell clusters fit into the nozzle, the bioink can be well extruded into 3D constructs. It is worth mentioning that the cell content in the bioink would also affect extrusion and printability. To verify this, we changed the cell concentration of S-Cell within the bioink. As shown in supplementary figure 3, increasing cell content could lead to clogging, non-uniform, or broken filament, destabilizing the printing process. The cell content of 0.12 g ml^{-1} and 0.06 g ml^{-1} yielded considerable uniform filaments. Drawing from existing research in plant cell bioprinting (supplementary table 1), it is evident that the cell content within bioink typically





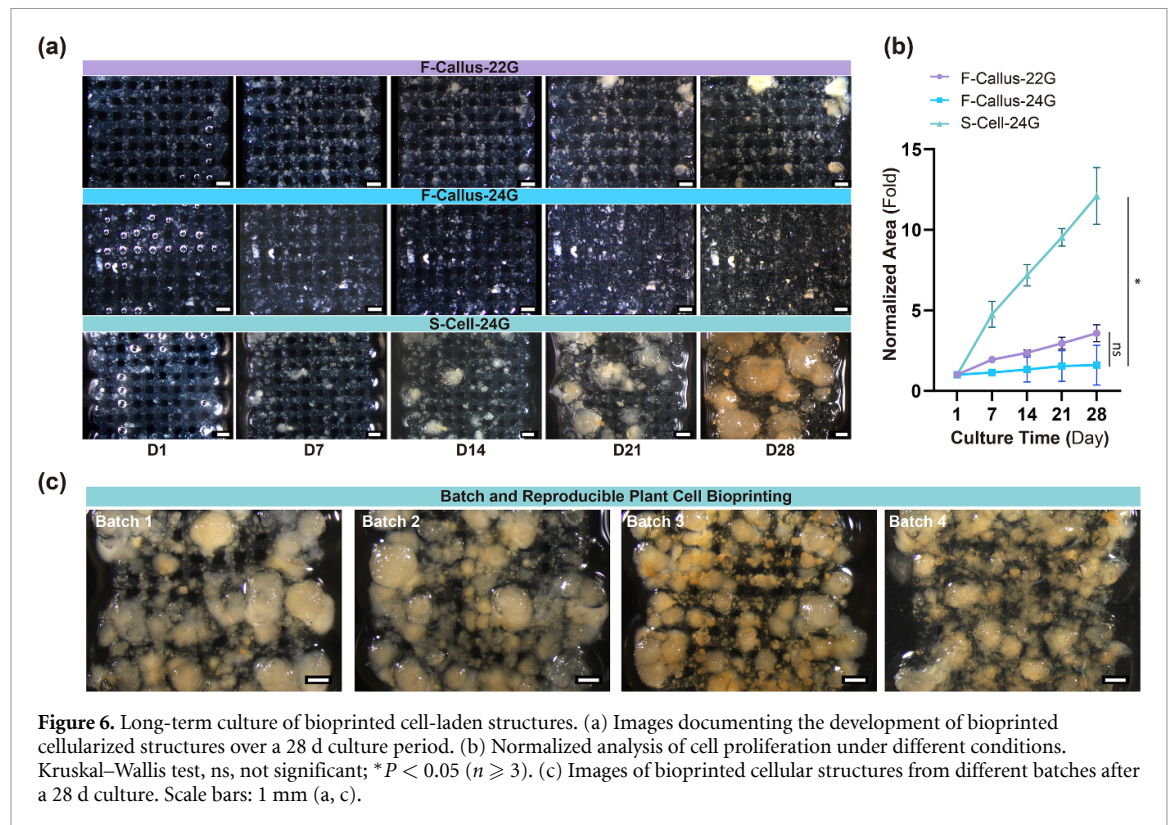
exceeds 10%. Given the similar widths of bioprinted filaments observed between bioinks with cell contents of 0.12 g ml^{-1} and 0.06 g ml^{-1} (supplementary figure 3), we fixed the cell content to 0.12 g ml^{-1} for all subsequent experiments. Next, we focused on harnessing cell cluster size and the selection of nozzles to balance printing resolution and cell viability.

Extrusion-based 3D bioprinting is suitable for fabricating heterogeneous constructs, which can be readily achieved by printing multiple materials with different printing nozzles. To demonstrate the feasibility of gelatin/alginate composite hydrogel in multi-nozzle printing of plant cells, we designed a carrot-shaped structure with green-labeled ‘leaves’ and red-labeled ‘root’ as a proof of concept (figure 4(g)). This structure was printed in a suspension bath that possesses a self-healing behavior, enabling freeform printing of complex structures. After crosslinking, the

resultant carrot structure displayed certain elasticity, allowing recovery post-compression (supplementary movie 1).

2.4. Cell viability and growth after bioprinting

To evaluate the viability of plant cells, we utilized a Live/Dead™ staining assay for the cells and those embedded in the bioprinted structures. Despite our efforts to mitigate the influence on cell viability by shearing the callus with nozzles of progressively decreasing diameter, considerable dead cells could be observed around the fragmented callus clusters, while the S-Cell group exhibited fewer dead cells (figure 5(a)). To quantify the viability of the plant cells, we approximated the ratio of green area (live cells) to the total area of green and red (dead cells), representing the relative cell viability. As shown in figure 5(b), cell viability is $81.4 \pm 8.6\%$ in the F-Callus



group and $89.2 \pm 2.6\%$ in the S-Cell group, with significant differences. Post-bioprinting cell viability was further evaluated on day 0 and day 4, revealing over 60%–70% cell viability on day 0 with an increasing proportion of live cells by day 4 ($\sim 80\%$) (figures 5(c) and (d)). The results showed that cells in the F-Callus-22G and S-Cell-24G groups exhibited slightly higher viability than those in the F-Callus-24G group. The larger cell cluster sizes within the F-Callus bioink might induce higher shear force in narrow needles (figure 4(f)). We further monitored the cell viability during a 35 d culture (figure 5(e)). Cells maintained a considerable viability and the size of cell clusters became larger with time. However, when assessing the bioprinting of S-Cell bioink using different nozzles, a significant difference in cell viability was noted between the largest 18G nozzle ($96.3 \pm 1.6\%$) and the narrowest 27G nozzle ($48.9 \pm 14.8\%$) (supplementary figure 2(c)). These results underscored the negative impact of shear forces during bioprinting on plant cells and, consequently, highlighted the importance of balancing appropriate cell sizes and nozzle diameters to maintain cell viability. The initial cell damage might be caused by the shearing force during extrusion, while the plant cells can rapidly revert to a high level of viability, similar to those without printing. The reduction of living cells and growing cells in the F-Callus-22G and F-Callus-24G groups on day 4 may be related to programmed cell death induced by non-lethal shear stress [22, 23]. In contrast, the number of living cells seemed to increase well in the S-Cell-24G group on day 4 (figure 5(c)).

We also studied the influence of cell content on cell viability after 24G-nozzle bioprinting. The cell viability results indicated a slight increase in cell viability with the decrease of cell content, though no significant differences were observed (figure 5(f)). This may be associated with the loose structure of suspension cell clusters, allowing for certain deformation to alleviate the shearing-induced damage as the cells pass through the nozzles.

We further employed bright-field images to record the bioprinted lattices and assess cell growth (figure 6(a)). The S-Cell-24G group showed robust growth, with macroscopic cell clusters visible from day 7. In contrast, much smaller clusters were observed in the F-Callus-22G group, and it was hard to identify the growth of clusters in the F-Callus-24G group. We conducted a quantitative analysis of cell growth by normalizing the area of cell clusters on different days to that on day 0 (figure 6(b)). After 28 d culture, the area of cell clusters expanded 3.6 ± 0.5 fold, 1.6 ± 1.2 fold, and 12.1 ± 1.8 fold in the F-Callus-22G, F-Callus-24G, and S-Cell-24G groups, respectively. The significant increase in the S-Cell-24G group confirmed the rapid cell growth. Combining these results with printability outcomes (figure 4), we can appreciate the importance of selecting the appropriate nozzle gauge and corresponding cell clusters to achieve good 3D printability and cell viability.

To further verify the reproducibility of bioprinting the S-Cell bioink, we carried out four independent bioprinting and culturing experiments for

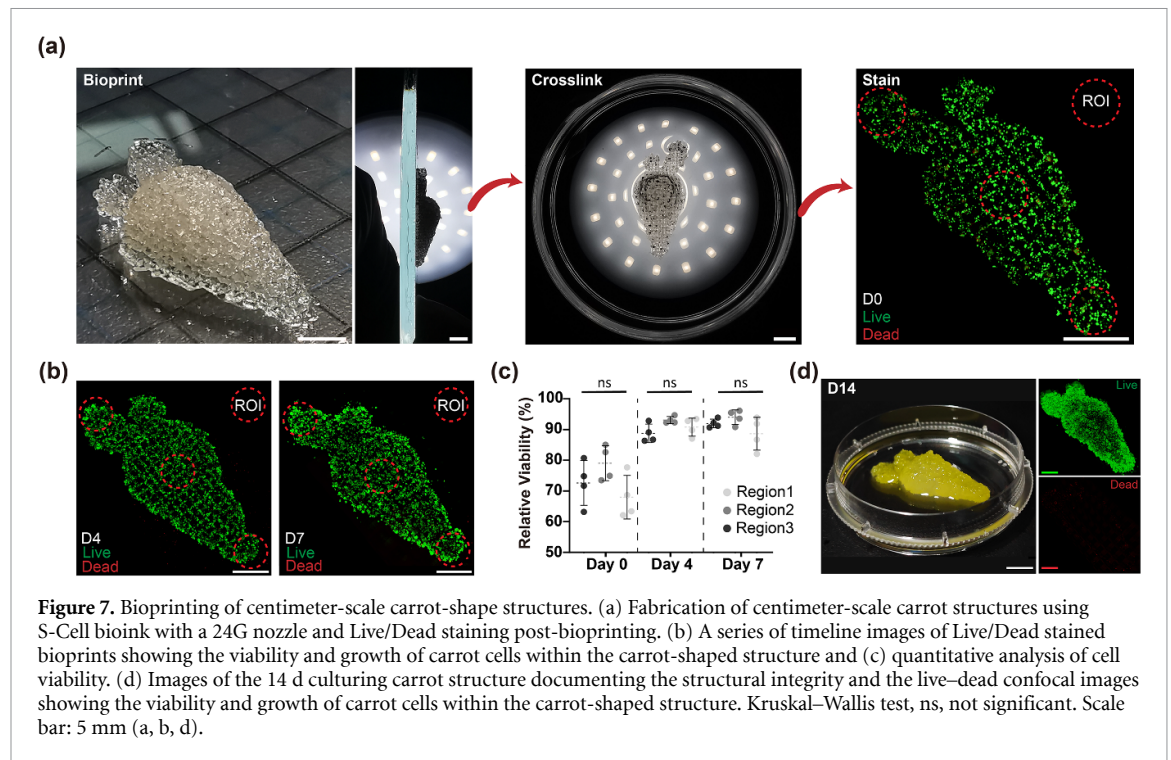


Figure 7. Bioprinting of centimeter-scale carrot-shaped structures. (a) Fabrication of centimeter-scale carrot structures using S-Cell bioink with a 24G nozzle and Live/Dead staining post-bioprinting. (b) A series of timeline images of Live/Dead stained bioprints showing the viability and growth of carrot cells within the carrot-shaped structure and (c) quantitative analysis of cell viability. (d) Images of the 14 d culturing carrot structure documenting the structural integrity and the live–dead confocal images showing the viability and growth of carrot cells within the carrot-shaped structure. Kruskal–Wallis test, ns, not significant. Scale bar: 5 mm (a, b, d).

28 d (figure 6(c)). Scaffolds from different batches all maintained their structure while exhibiting desirable cell growth over a 28 d culture, providing strong evidence of reproducibility in both printability and cell activity. Although the gelatin might escape from the hydrogel during culture due to its uncrosslinked status [24], the bioprinted structures well maintained the integrity. We also observed that some cell clusters would continue to grow throughout the scaffold (figure 6(c)), which was also reported in the bioprinting of mammalian cells [25]. In general, the gelatin/alginate composite hydrogel has proven to be competent to support long-term culture of carrot cells.

2.5. 3D printing of large-scale plant model

In the scenario of printing large-scale models, there is a risk of nutrition shortage for cells due to the prolonged printing duration. To address this, we fortified the hydrogel formulation with sucrose, a nutrient for plant cells. We created a centimeter-sized carrot-shaped structure and performed the printing using S-Cell bioink and a 24G nozzle (figure 7(a)). Leveraging the self-supporting properties of the hydrogel, the bioink was deposited layer-by-layer on a flat platform. The crosslinking agent, supplemented with sucrose, enables rapid crosslinking of the hydrogel in a few minutes. The results demonstrated the structural integrity of the centimeter-scale construct with distinct substructures, and cells displayed considerably high viability and uniform distribution after bioprinting. As shown in figure 7(b), living cells were uniformly distributed within the carrot-shaped structure, with increasing size as the culture time grew. The results revealed that cell viability rose to a high

level (>80%) after a 7 d culture period and maintained after a 14 d culture period (figures 7(c) and (d)). These results suggest that the permeability of the gel-based scaffolds is sufficient to support cell growth within centimeter-scale structures.

We further performed gene sequencing to determine the gene expression of bioprinted cells (Bioprint, collected after 7 d of culturing) and non-bioprinted cells (Control), as evidenced by hierarchical clustering of differentially expressed genes (DEGs). 16.5% of the genes showed significant differential expression, with 3002 genes upregulated and 1159 genes downregulated in the bioprinted group (figure 8(a)). Gene Ontology (GO) enrichment analysis which was conducted to categorize the functions of these DEGs, revealed significant shifts in both upregulated and downregulated fields, offering a deeper understanding of the cellular response to the bioprinting process (figure 8(b)). Genes associated with cell recognition, cell wall organization or biogenesis, defense response, and oxidative stress response were significantly enriched in the bioprinting group, suggesting activation of stress adaptation mechanisms, including structural reinforcement and antioxidant defenses. Conversely, the downregulation of carbohydrate metabolism pathways (e.g. glycolysis and sucrose metabolism), along with nitrogen metabolism, may reflect a shift in the plant's metabolic state, reallocating resources from primary metabolism to stress response and repair. The Kyoto Encyclopedia of Genes and Genomes (KEGG) enrichment analysis (figure 8(c)) confirmed the upregulation of pathways such as phenylpropanoid biosynthesis [27], crucial for lignin and cell

Along with producing secondary metabolites, researchers have already attempted to generate tunable plant-based material with customized shapes [10, 11]. Concurrently, decellularized plant-derived scaffolds have emerged as a novel approach in tissue engineering, directing mammalian cell behaviors [33]. The convergence of plant and mammalian cell bioprinting presents an intriguing and potentially transformative technique to modulate tissue formation in tissue engineering, enhancing meat production, and even creating unprecedented plant-meat hybrid foods. However, the behavior of plant cells within 3D hydrogel structures and the underlying mechanisms requires further exploration to foster the development of these applications.

4. Materials and methods

4.1. Materials

Carrot Callus Initiation Basal medium, Murashige & Skoog (MS) Basal medium, 2,4-dichlorophenoxyacetic acid, and Kinetin were purchased from Phytotech (USA). Gelatin with a gel strength of ~ 240 g, sodium alginate, and anhydrous calcium chloride were purchased from Aladdin (China). Sucrose and agar powder were acquired from Solarbio (China). Carrots (*Daucus carota* L.) were sourced from a local market (China). Fluorescein diacetate was purchased from Coolaber (China) and propidium iodide was purchased from KeyGEN (China).

4.2. Carrot cell culture

We generated callus and suspension cells by developing a protocol based on previous reports [12, 34]. As shown in figure 1, carrot callus culture was initiated from explants of fresh carrots, which were thoroughly rinsed to eliminate surface impurities, cut into discs, and surface-sterilized in a clean bench environment. Then, the explants were placed on a solid medium composed of Carrot Callus Initiation Basal Medium supplemented with 3 wt% sucrose, 0.8 wt% agar powder, 1 mg l^{-1} 2,4-dichlorophenoxyacetic acid, and 0.5 mg l^{-1} Kinetin, with pH adjusted to 5.8 ± 0.1 . After 4 weeks' incubation in darkness at 25°C , the induced callus was transferred to the fresh solid medium. Healthy callus was screened and sub-cultured every 4 weeks over 4 months to establish a stable callus supply for the subsequent experiments. For the suspension culture, 3 g of calli was suspended in flasks containing 50 ml liquid MS Basal medium supplemented with 3 wt% sucrose, 1 mg l^{-1} 2,4-dichlorophenoxyacetic acid, and 0.5 mg l^{-1} Kinetin with pH adjusted to 5.8 ± 0.1 . The cells were passaged every 4 d by transferring 20 vol% of cell suspension to 80 vol% fresh liquid medium. All liquid cultures for suspension cells and bioprinted structures in this study were maintained on an orbital rotary shaker

(100 rpm, 15 mm shaking diameter) at room temperature ($25 \pm 1^\circ\text{C}$) in darkness. To ensure the homogeneity of the suspension cells to be used in bioprinting, we used the cells at passage 6 or 7.

4.3. Bioink preparation

The bioinks were formulated using hydrogel precursor solution and plant cells. The hydrogel precursor stock solution was prepared by dissolving 20 wt% gelatin, 3 wt% sucrose, and 3 wt% sodium alginate in distilled water. A crosslinking agent was prepared by dissolving 3 wt% calcium chloride (CaCl_2) and 3 wt% sucrose in distilled water. All solutions were sterilized via pasteurization and then stored at 4°C until use. For the preparation of the callus solution at a concentration of 0.24 g ml^{-1} , 2.4 g regular callus was suspended and homogenized in 10 ml liquid medium and subsequently aliquoted into two sterile tubes. One aliquot was subjected to a series of extrusion treatments using 18G, 22G, and 24G nozzles to progressively reduce the callus cluster size, leading to the F-Callus group. The other aliquot remained untreated as the R-Callus group. For the preparation of the suspension cells solution at a concentration of 0.24 g ml^{-1} , the suspension cells were collected and centrifuged at 800 g for 5 min. After carefully removing the supernatant, the cell pellet was weighed and resuspended in an appropriate volume of liquid medium to achieve the target cell density. Finally, these cell-containing solutions were mixed with hydrogel precursor stock solution in a 1:1 volume ratio to create distinct bioink formulations.

4.4. Diameter analysis of cell clusters and optical analyses of bioink

To quantify the diameter of cell clusters, we randomly captured images of three solutions containing with regular callus (R-Callus), fragmented callus (F-Callus), and suspension cells (S-Cell) using an optical microscope (CKX53, Olympus, Japan). The diameters of the cell clusters were measured using ImageJ software (National Institutes of Health, USA). Further, a laser particle analyzer (Mastersizer 3000, Malvern Panalytical, UK) was used to determine the size and distribution of the cell clusters. To verify the transparency of the cellular bioinks, we photographed the gelled samples positioned over a background of white paper with black letters. Additionally, the OD value of these bioinks in both liquid and gel states was measured using a microplate reader (Thermo Fisher Scientific, America) at wavelengths of 450 nm.

4.5. Rheological measurement

The rheological tests were conducted using an MCR 302 rheometer (Anton Paar, Austria) with a parallel plate (PP25) to characterize the viscosity, shear-thinning behavior, thermosensitivity, and self-healing properties of different bioink formulations. The gap distance was standardized to 0.5 mm, and

300 μl solutions were prepared for each test. To assess the viscosity and shear-thinning property, rotational experiments were performed with a shear rate ranging from 0.01 to 10 s^{-1} . To evaluate the thermo-sensitivity, a temperature sweep from 30 $^{\circ}\text{C}$ to 4 $^{\circ}\text{C}$ in oscillation mode (1% strain, 1.5 Hz) was performed to monitor the storage (G') and loss modulus (G'') over time. The self-healing capacity was assessed using high (1000%) and low (1%) strain cycle oscillatory tests (1.5 Hz) on the samples gelled at 18 $^{\circ}\text{C}$.

4.6. Extrusion experiments

The extrusion experiments and bioprinting were conducted using the mechanical-driven 3D bioprinter (SUNP Biomaker 2, China) to standardize extrusion conditions. Briefly, three independent bioinks were transferred into separate syringes and loaded into the bioprinter. The temperature of cartridge was set at 18 ± 1 $^{\circ}\text{C}$ and the extrusion speed was uniformly set to 0.8 ml min^{-1} . Following a 15-min incubation, the bioink was extruded through a series of nozzles with gauges 18G, 22G, 24G, and 27G. The process of filament extrusion was captured by a camera, and the maximum length of hanging filament was measured.

4.7. Bioprinting

The lattice scaffolds were designed as $10 \times 10 \times 1.2$ mm square grids and printed using nozzles of 18G, 22G, 24G, and 27G gauges. The specific printing parameters are listed in supplementary table 2. The temperature of platform and cartridge was controlled at 15 ± 1 $^{\circ}\text{C}$ and 18 ± 1 $^{\circ}\text{C}$, respectively. After printing, the scaffolds were immersed into a 3 wt% CaCl_2 solution for 3 min to crosslink the alginate. Then all the cell-laden scaffolds were washed twice with liquid medium to remove the crosslinking agent and then supplied with liquid medium for long-term culture. For the fabrication of complex structures, S-Cell bioink was employed with a 24G nozzle to print the carrot-shaped models. The temperature of cartridge was set at 25 $^{\circ}\text{C}$ for printing in the suspension bath to maintain the well-flowable state of the bioink.

4.8. Cell viability and growth

Cell viability was assessed using the Fluorescein diacetate/Propidium Iodide stain solution. Following a 5-min incubation at 25 $^{\circ}\text{C}$ in dark, the cellular samples were photographed using a confocal fluorescence microscope (FV3000, Olympus, Japan). The area of green (live) and red (dead) cells was measured by image J. The ratio of green cell area to the sum of green and red cells was determined to be the cell viability. A multi-modal confocal system (Dragonfly 200, Andor, UK) was used to create a fluorescent panorama of scaffolds. Optical images of scaffolds were photographed under a stereoscopic microscope (SMZ745, Nikon, UK) to record the cell growth.

4.9. RNA-seq expression analysis

RNA concentration and integrity were assessed using the RNA Nano 6000 Assay Kit of the Bioanalyzer 2100 system (Agilent Technologies, CA, USA). Messenger RNA was purified from total RNA using poly-T oligo-attached magnetic beads for sequencing libraries generation. The library was checked with Qubit and real-time PCR for quantification and bioanalyzer for size distribution detection. After library quality control, different libraries were pooled based on the effective concentration and targeted data amount, then subjected to Illumina sequencing. Fluorescence signals were recorded and converted into sequencing peaks for differential expression analysis, including Gene Ontology (GO) and KEGG enrichment analysis using the clusterProfiler R package. Differentially expressed genes (DEGs) were identified using $|\log_2\text{FoldChange}| \geq 1$ and $P_{\text{adj}} \leq 0.05$ as thresholds. Only genes with significant functional annotation or enrichment in GO terms or KEGG pathways were included in the analysis.

4.10. Statistical analysis

All the experiments were independently repeated at least three times, and the data was presented as the mean \pm the standard deviation. The statistical analysis was executed using GraphPad Prism 9.5 (USA). All statistical comparisons employed were detailed in the corresponding figure captions. A value of $P < 0.05$ was considered statistically significant.

Data availability statement

All data that support the findings of this study are included within the article (and any supplementary files).

Acknowledgment

This work is supported by the National Natural Science Foundation of China (Nos. 32211530075, 52105306), the 111 Project of the State Administration of Foreign Experts Affairs of China (B17026), and Faculty Startup Funding from Tsinghua University (012-533302004). The authors acknowledge the help from Changming Yang for cell culture and Weiyi Rao for imaging. L O acknowledges the general support from Dr W Sun, Dr Z Xiong, Dr F Lin, Dr T Zhang, and Dr L Zhang.

Conflict of interest

The authors declare that they have no competing interests.

ORCID iDs

Dezhi Zhou(周德志)  <https://orcid.org/0000-0002-6739-3510>

Shuang Yu(余爽)  <https://orcid.org/0009-0006-0483-8160>

Liliang Ouyang(欧阳礼亮)  <https://orcid.org/0000-0003-4177-8698>

References

- [1] Lindsey K and Yeoman M M 1987 [36] Techniques for the immobilization of plant cells *Methods Enzymol.* **135** 410–21
- [2] Dörnenburg H and Knorr D 1995 Strategies for the improvement of secondary metabolite production in plant cell cultures *Enzyme Microb. Technol.* **17** 674–84
- [3] Gilleta F, Roisin C, Fliniaux M A, Jacquín–Dubreuil A, Barbotin J N and Nava–Saucedo J E 2000 Immobilization of *Nicotiana tabacum* plant cell suspensions within calcium alginate gel beads for the production of enhanced amounts of scopolin *Enzyme Microb. Technol.* **26** 229–34
- [4] Wilson S A and Roberts S C 2012 Recent advances towards development and commercialization of plant cell culture processes for the synthesis of biomolecules *Plant Biotechnol. J.* **10** 249–68
- [5] Lode A, Krujatz F, Brüggemeier S, Quade M, Schütz K, Knaack S, Weber J, Bley T and Gelinsky M 2015 Green bioprinting: fabrication of photosynthetic algae-laden hydrogel scaffolds for biotechnological and medical applications *Eng. Life Sci.* **15** 177–83
- [6] Krujatz F, Lode A, Brüggemeier S, Schütz K, Kramer J, Bley T, Gelinsky M and Weber J 2015 Green bioprinting: viability and growth analysis of microalgae immobilized in 3D-plotted hydrogels versus suspension cultures *Eng. Life Sci.* **15** 678–88
- [7] Seidel J, Ahlfeld T, Adolph M, Kümmeritz S, Steingroewer J, Krujatz F, Bley T, Gelinsky M and Lode A 2017 Green bioprinting: extrusion-based fabrication of plant cell-laden biopolymer hydrogel scaffolds *Biofabrication* **9** 045011
- [8] Wang Y J, Di Z, Qin M, Qu S, Zhong W, Yuan L, Zhang J, Hibberd J M and Yu Z 2024 Advancing engineered plant living materials through tobacco BY-2 cell growth and transfection within tailored granular hydrogel scaffolds *ACS Cent. Sci.* **10** 1094–104
- [9] Varma A, Gemeda H B, McNulty M J, McDonald K A, Nandi S and Knipe J M 2021 Immobilization of transgenic plant cells towards bioprinting for production of a recombinant biodefense agent *Biotechnol. J.* **16** e2100133
- [10] Beckwith A L, Borenstein J T and Velásquez-García L F 2022 Physical, mechanical, and microstructural characterization of novel, 3D-printed, tunable, lab-grown plant materials generated from cell cultures *Mater. Today* **54** 27–41
- [11] Beckwith A L, Borenstein J T and Velásquez-García L F 2021 Tunable plant-based materials via *in vitro* cell culture using a *Zinnia elegans* model *J. Clean. Prod.* **288** 125571
- [12] Park S M, Kim H W and Park H J 2020 Callus-based 3D printing for food exemplified with carrot tissues and its potential for innovative food production *J. Food Eng.* **271** 109781
- [13] Vancauwenbergh V, Baiye Mfortaw Mbong V, Vanstreels E, Verboven P, Lammertyn J and Nicolai B 2019 3D printing of plant tissue for innovative food manufacturing: encapsulation of alive plant cells into pectin based bio-ink *J. Food Eng.* **263** 454–64
- [14] Van den Broeck L et al 2022 Establishing a reproducible approach to study cellular functions of plant cells with 3D bioprinting *Sci. Adv.* **8** eabp9906
- [15] Emmermacher J, Spura D, Cziommer J, Kilian D, Wollborn T, Fritsching U, Steingroewer J, Walther T, Gelinsky M and Lode A 2020 Engineering considerations on extrusion-based bioprinting: interactions of material behavior, mechanical forces and cells in the printing needle *Biofabrication* **12** 025022
- [16] Namdev P K and Dunlop E H 1995 Shear sensitivity of plant-cells in suspensions—present and future *Appl. Biochem. Biotechnol.* **54** 109–31
- [17] Sowana D D, Williams D R G, Dunlop E H, Dally B B, O’Neill B K and Fletcher D F 2001 Turbulent shear stress effects on plant cell suspension cultures *Chem. Eng. Res. Des.* **79** 867–75
- [18] Li S-F, Ye T-W, Xu X, Yuan D-Y and Xiao S-X 2021 Callus induction, suspension culture and protoplast isolation in *Camellia oleifera* *Sci. Hort.* **286** 110193
- [19] Zhou D Z, Dou B, Kroh F, Wang C and Ouyang L 2023 Biofabrication strategies with single-cell resolution: a review *Int. J. Extreme Manuf.* **5** 042005
- [20] Rafe A and Razavi S M A 2017 Scaling law, fractal analysis and rheological characteristics of physical gels cross-linked with sodium trimetaphosphate *Food Hydrocoll.* **62** 58–65
- [21] Manojlovic V, Djonlagic J, Obradovic B, Nedovic V and Bugarski B 2006 Investigations of cell immobilization in alginate: rheological and electrostatic extrusion studies *J. Chem. Technol. Biotechnol.* **81** 505–10
- [22] Hua J, Erickson L E, Yiin T-Y and Glasgow L A 1993 A review of the effects of shear and interfacial phenomena on cell viability *Crit. Rev. Biotechnol.* **13** 305–28
- [23] Galluzzi L et al 2015 Essential versus accessory aspects of cell death: recommendations of the NCCD 2015 *Cell Death Differ.* **22** 58–73
- [24] Ouyang L L, Armstrong J P K, Lin Y, Wojciechowski J P, Lee-Reeves C, Hachim D, Zhou K, Burdick J A and Stevens M M 2020 Expanding and optimizing 3D bioprinting capabilities using complementary network bioinks *Sci. Adv.* **6** eabc5529
- [25] Ouyang L L, Yao R, Mao S, Chen X, Na J and Sun W 2015 Three-dimensional bioprinting of embryonic stem cells directs highly uniform embryoid body formation *Biofabrication* **7** 044101
- [26] Lu L, Zhang Y, Li L, Yi N, Liu Y, Qaseem M Faisal, Li H, Wu A 2021 Physiological and Transcriptomic Responses to Nitrogen Deficiency in *Neolamarckia cadamba* *Front Plant Sci* **12** 747121
- [27] Dong N-Q and Lin H-X 2021 Contribution of phenylpropanoid metabolism to plant development and plant–environment interactions *J. Integr. Plant Biol.* **63** 180–209
- [28] Wu J, Lv S, Zhao L, Gao T, Yu C, Hu J and Ma F 2023 Advances in the study of the function and mechanism of the action of flavonoids in plants under environmental stresses *Planta* **257** 108
- [29] Manna M, Rengasamy B and Sinha A K 2023 Revisiting the role of MAPK signalling pathway in plants and its manipulation for crop improvement *Plant Cell Environ.* **46** 2277–95
- [30] Krasteva G, Georgiev V and Pavlov A 2021 Recent applications of plant cell culture technology in cosmetics and foods *Eng. Life Sci.* **21** 68–76
- [31] Mehrotra S, Kumar S, Srivastava V, Mishra T and Mishra B N 2020 3D bioprinting in plant science: an interdisciplinary approach *Nat. Protocols* **25** 9–13
- [32] Stavrinidou E, Gabrielsson R, Gomez E, Crispin X, Nilsson O, Simon D T and Berggren M 2015 Electronic plants *Sci. Adv.* **1** e1501136
- [33] Shang L, Wang S and Mao Y 2024 Recent advances in plant-derived polysaccharide scaffolds in tissue engineering: a review *Int. J. Biol. Macromol.* **277** 133830
- [34] Mustafa N R, de Winter W, van Iren F and Verpoorte R 2011 Initiation, growth and cryopreservation of plant cell suspension cultures *Nat. Protocols* **6** 715–42